Three-Dimensional Analysis of the Effect of Epidermal Growth Factor on Cell-Cell Adhesion in Epithelial Cell Clusters

J. Notbohm,[†*] J. -H. Kim,[‡] A. R. Asthagiri,[§] and G. Ravichandran[†]
[†]California Institute of Technology, Pasadena, California; [‡]Gwangju Institute of Science and Technology, Gwangju, South Korea; and [§]Northeastern University, Boston, Massachusetts

ABSTRACT The effect that growth factors such as epidermal growth factor (EGF) have on cell-cell adhesion is of interest in the study of cellular processes such as epithelial-mesenchymal transition. Because cell-cell adhesions cannot be measured directly, we use three-dimensional traction force microscopy to measure the tractions applied by clusters of MCF-10A cells to a compliant substrate beneath them before and after stimulating the cells with EGF. To better interpret the results, a finite element model, which simulates a cluster of individual cells adhered to one another and to the substrate with linear springs, is developed to better understand the mechanical interaction between the cells in the experiments. The experiments and simulations show that the cluster of cells acts collectively as a single unit, indicating that cell-cell adhesion remains strong before and after stimulation with EGF. In addition, the experiments and model emphasize the importance of three-dimensional measurements and analysis in these experiments.

INTRODUCTION

Epithelial cells organize into multicellular structures by establishing highly structured adhesions with their neighbors and the surrounding extracellular matrix (ECM) (1). During morphogenesis, cells continuously sense cues in their microenvironment, such as ECM ligands and soluble growth factors, and respond by modulating their adhesions, cytoskeletal mechanics, and cell shape (2). These biophysical changes in turn affect intracellular signal transduction and control many cellular behaviors including proliferation and migration. Thus, deciphering how these environmental cues control multicellular mechanics and spatial patterns in cell shape and proliferation is central to our understanding of multicellular morphodynamics.

Exposure to soluble growth factors can affect cellular protrusions and actomyosin contractility, which in turn affect cellular behavior and mechanics. For example, it was found that clusters of MCF-10A cells maintain contact inhibition of proliferation at a low concentration of epidermal growth factor (EGF) while they undergo contact-independent growth at a higher concentration of EGF (3,4). In addition, clusters of epithelial cells that are exposed to particular growth factors can undergo an epithelial-mesenchymal transition (EMT)-like process (5) with some cell types exhibiting decompaction while still nominally maintaining cell-cell contacts (3) and others undergoing cell scattering. An example is the work by de Rooij et al. (6), who found that the hepatocyte growth factor causes cell-cell adhesion disruption and cell scattering in a process similar to EMT. In addition, it has been demonstrated that EGF can activate EMT in cancer cells (7).

For the processes of cluster decompaction and scattering to occur, the cells must first reduce their adhesions with one another, either partially in the case of decompaction or more completely in the case of cell scattering. The precise mechanism for the reduction in cell-cell adhesion still remains to be elucidated. It is known that EGF stimulates the membrane translocation of Rac1 and its localized activation (8), facilitating lamellipodial extensions. Meanwhile, EGF also activates the Rho GTPase effector, ROCK, leading to the phosphorylation of myosin-II regulatory light chains and inactivation of myosin-II phosphatases, which together give rise to the increased nonmuscle myosin II-mediated contractility (9). In isolated cells, these mechanisms are associated with the formation of new adhesions at the leading edge and the destabilization of focal adhesions at the trailing edge, together driving cell migration. However, in multicellular clusters, the mechanics of the cell-cell bonding adds an extra layer of complexity to the system. A current open question is whether EGF signals cells to downregulate expression of E-cadherin, a membrane protein associated with cell-cell adhesion. In Madin-Darby canine kidney cell clusters, it has been found that E-cadherin expression is not downregulated by EGF (6); however, in cancerous CaSki and SiHa cell clusters, EGF has been shown to reduce E-cadherin expression (7).

Modulating E-cadherin expression is just one way of regulating cell-cell adhesions. Phosphorylation of E-cadherin and β-catenin can modulate E-cadherin/β-catenin binding in addition to affecting the synthesis and turnover of E-cadherin (10,11). Furthermore, the formation and maturation of adherens junctions depends on other proteins, such as Merlin, that associate with α-catenin, an actin-binding protein (12). Finally, E-cadherin-based adherens junctions are not the sole mediators of cell-cell adhesion. Other types of adhesions, such as tight junctions mediated

Submitted November 28, 2011, and accepted for publication February 13, 2012.

*Correspondence: notbohm@caltech.edu

Editor: Denis Wirtz.

0006-3495/12/03/1323/8 $2.00

doi: 10.1016/j.bpj.2012.02.016

by ZO-1, also contribute to cell-cell adhesion (13). The intricate molecular assemblies mediating cell-cell adhesion further motivate the need for a more integrative, quantitative readout of the effect of EGF on cell-cell adhesion mechanics such as a mechanical measurement of the forces associated with cell-cell and cell-substrate adhesion.

To address the response of cell tractions to EGF, the technique of three-dimensional (3D) traction force microscopy (TFM) is applied to clusters of MCF-10A cells before and after stimulation with EGF. A simple mechanical model that makes use of a finite element simulation is then applied to better understand the way in which MCF-10A cells interact in a cluster and adhere to substrate beneath them.

EXPERIMENTAL METHODS

Cell culture

MCF-10A cells were cultured in DME medium/Ham's F-12 (Invitrogen, Carlsbad, CA) containing HEPES and L-glutamine supplemented with 5% (v/v) horse serum (Invitrogen), 20 ng/mL EGF (Peprotech, Rocky Hill, NJ), 0.5 μg/mL hydrocortisone, 0.1 μg/mL cholera toxin, 10 μg/mL insulin (Sigma-Aldrich, St. Louis, MO), and 1% penicillin-streptomycin (Invitrogen). For experiments, cells were seeded on fibronectin-coated polyacrylamide gels and grown in the complete medium for 24 h. Before imaging, cells were serum starved for an additional 24 h and labeled with 200 nM of Mitotracker Deep Red (Invitrogen) for 15 min.

Preparation of polyacrylamide gels

Polyacrylamide gels were made with 10% polyacrylamide (Bio-Rad Laboratories, Hercules, CA) and 0.04% bisacrylamide (Bio-Rad Laboratories). To image the displacements of the polyacrylamide substrates, 1 μm fluorescent polystyrene particles (Invitrogen Yellow-Green Fluorescent FluoSpheres) were added to the gels to a final volume concentration of ~0.2%. The elastic properties of the polyacrylamide substrates were measured by performing a stress-relaxation experiment with a compression device (14) on specimens made separately with an approximate diameter of 10 mm and an approximate height of 5 mm. It was found that the constitutive behavior of the polyacrylamide gels was well-approximated by using the linear, elastic form of Hooke's law. The Young's modulus of the material was chosen such that it was low enough for the cells to apply a noticeable displacement to the substrate, but high enough for the cells in each cluster to remain in a monolayer instead of resting on one another. It was found that a value of Young's modulus of (mean $\pm$ standard deviation) 7.1 $\pm$ 0.4 kPa met this criterion. The polyacrylamide substrates were coated with the heterobifunctional cross-linker sulfo-SANPAH (Pierce, Rockford, IL). Fibronectin (Sigma-Aldrich) was then covalently bound to the polyacrylamide substrates by placing the substrates in a 100 μg/mL fibronectin solution overnight at 4°C.

Confocal microscopy

A C1 confocal microscope on a TE2000 stand (Nikon Instruments, Melville, NY) was used with a 60× 1.45 NA oil immersion objective (Nikon Instruments). A 488 nm argon laser and a 633 nm helium-neon laser were used to excite fluorescence of the fluorescent particles and cell dye, respectively. 512 × 512 pixel images were collected in a field of view of 200 × 200 μm^2. A 20 μm confocal stack was collected with a step size of 0.2 μm. Next, EGF (Peprotech) was introduced into the cell media at a concentration of 100 ng/mL. Additional volume stacks were collected of the cell clusters and underlying substrate 30 min and 90 min after stimulation with EGF. Finally, the cells were lysed with 0.5% Triton X-100 (Invitrogen), and a fourth volume stack was collected. All confocal imaging was performed at 37°C using a custom built enclosure heated with an Air-Therm ATX heater (World Precision Instruments, Sarasota, FL).

Displacement and traction computation

Because the confocal imaging resolution in the axial (z) direction was lower than in the in-plane (x-y) directions, the spherical fluorescent particles were imaged as ellipsoids that were elongated in the axial direction. To improve the axial resolution, the Lucy-Richardson deconvolution algorithm (15) was used to deconvolve the image stack from the axial point spread function of the confocal microscope.

To compute the tractions applied by the MCF-10A cell clusters to the polyacrylamide substrate, a digital volume correlation (DVC) algorithm (14) was first used to calculate the full 3D displacement profile within the substrate. This algorithm used the random speckle pattern created by the fluorescent particles within the substrate to compute the displacement of a 64 × 64 × 64 voxel subvolume by comparing how the particles displaced within the subvolume before and after deformation. The correlation was repeated for multiple subvolumes within the substrate at a separation of 8 voxels. The DVC algorithm accounted for both translations and stretches of the subvolume, but not rotations, so it was appropriate for small shear strains of $<$ ~5% (14).

After displacement computation, strains were calculated from the filtered displacement data by fitting a 3 × 3 × 3 window of grid points to a trilinear function to determine the displacement gradients as described previously (14). This method computed the strains directly from the displacement data, and it circumvented the need for an inverse-Boussinesq formulation that would require regularization (16) and additional analysis to account for the finite thickness of the substrate (17). Once the strain tensor was assembled, the stress tensor was computed from the incompressible form of Hooke's law. Because the technique of computing the stress tensor from the displacements through the strain tensor and constitutive law gave the 3D state of stress at any point within the material, the tractions applied by the cell cluster were easily calculated according to the Cauchy relation, $\mathbf{t} = \sigma \cdot \mathbf{n}$. In this equation, $\mathbf{t}$ was the traction vector, σ was the 3D stress tensor, and $\mathbf{n}$ was the unit vector normal to the substrate's surface. To compute the tractions applied by the cells, the traction vector was computed for each point on the top surface of the substrate. Because the traction vector was computed from the 3D stress tensor, both the in-plane (horizontal) and out-of-plane (vertical, or along the axis of the objective lens) components of the traction vector were computed using this technique.

The resolution of the DVC technique was determined by performing control experiments wherein a polyacrylamide gel with no cells was imaged before and after injecting Triton. Artificial strains in the range of 2% to 6% were applied computationally to one of the volume stacks to compute the resolution under loading. The displacement noise floor was found to range from 0.05 μm (for in-plane displacement components) to 0.10 μm (for out-of-plane displacement components). Upon differentiation, the strain noise floor was found to be ~1% for the out-of-plane (z) components of the strain tensor. Because displacements and strains smaller than the noise floor could not be resolved by DVC, values of displacement and strain that were measured to be smaller than the noise floor were set to zero for plotting and analysis. All experimental data computation and image processing were performed using MATLAB (The MathWorks, Natick, MA).

Finite element simulation

A simple finite element (FE) model (Fig. 1) was created in ABAQUS 6.9 (Simulia, Providence, RI) to simulate the contraction of a cell cluster on a compliant substrate. In the model, the substrate properties were chosen such that they matched the properties of the polyacrylamide gels that

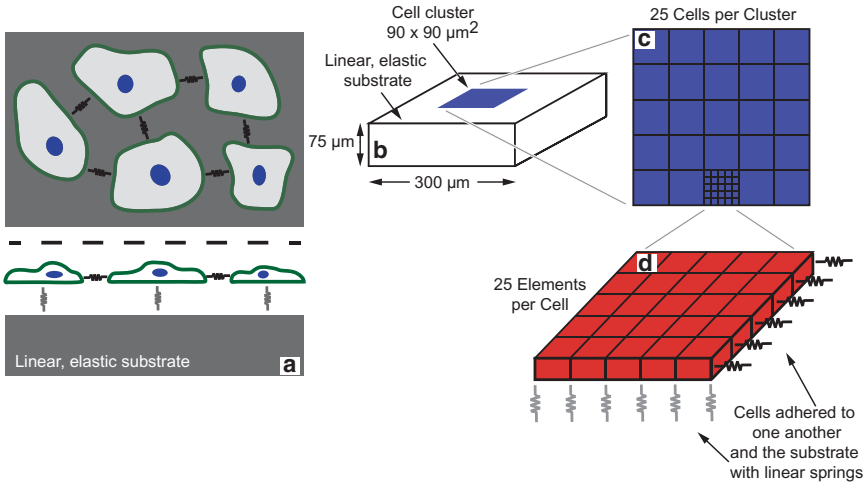

FIGURE 1 (*a*) Diagram of the FE model. The cells are adhered to one another and to the substrate with linear springs. (*b*) The geometry of the FE model. A 90 × 90 μm^2 cell cluster (Young's modulus E_{cell} = 1 kPa; Poisson's ratio ν_{cell} = 0.3) is placed on a linear, elastic substrate (Young's modulus $E_{substrate}$ = 7.1 kPa; Poisson's ratio $\nu_{substrate}$ = 0.48). (*c*) The cell cluster is composed of 25 cells. (*d*) Each cell is composed of 25 elements, is connected to neighboring cells with linear springs, and is connected to the substrate with a different set of linear springs at each node. A computational thermal strain is used to simulate the contraction of the cell cluster.

were used as substrates in the experiments: the substrate was modeled with linear, elastic 8-node brick elements with a Young's modulus of 7.1 kPa and a Poisson's ratio of 0.48. The cells were modeled as linear, elastic 8-node bricks with a Young's modulus of 1 kPa (19) and a Poisson's ratio of 0.3 (20). Each cell was composed of 25 brick elements. Following previous models for cellular adhesion (21,22), the cell elements were connected to the substrate by linear springs at each node. Additionally, the exterior nodes of each cell were connected to neighboring cell nodes with a different set of linear springs. In-plane contraction of the cells was modeled using a thermal strain in the cell elements. Because a cell on a substrate contracts the most in the in-plane (*x*-*y*) directions, the thermal contraction was applied only in the in-plane directions. Symmetric boundary conditions were used to model only a quarter of the geometry. In addition, a fixed boundary was applied at the bottom of the substrate.

In the FE model, three parameters required calibration, the spring stiffnesses associated with cell-cell and cell-substrate adhesion, and the amount of thermal strain applied to the cell cluster. The value of spring stiffness to be used can be better understood by dividing the spring stiffness by the distance between the springs, thus creating a quantity with units of force divided by area. This quantity is defined as the contact modulus $E_{contact}$. To relate $E_{contact}$ to the cell elements' Young's modulus, E_{cell}, a dimensionless parameter that quantifies the adhesion stiffness is defined: $\kappa = E_{contact}/E_{cell}$. Because there are two sets of springs, one set for the cell-cell adhesions and one for the cell-substrate adhesions, two values of κ are used, and they are called $\kappa_{cell\text{-}cell}$ and $\kappa_{cell\text{-}substrate}$, respectively. Using the previous definition, the lower bound for both $\kappa_{cell\text{-}cell}$ and $\kappa_{cell\text{-}substrate}$ is zero. An approximate upper bound for $\kappa_{cell\text{-}cell}$ and $\kappa_{cell\text{-}substrate}$ was set to 1, because increasing the contact stiffness greater than the Young's modulus of the cell was not expected to have a noticeable effect on the tractions applied by the contractile layer to the substrate. To test this upper bound, a value for $\kappa_{cell\text{-}cell}$ of 10 was used, and the results were not noticeably different than the approximate upper bound of 1. To determine the lower bound of $\kappa_{cell\text{-}cell}$, the FE model was solved with values of $\kappa_{cell\text{-}cell}$ ranging from 0.01 to 1. It was found that the root mean-square (RMS) and maximum tractions changed by only 10% when changing $\kappa_{cell\text{-}cell}$ from 0.01 to 0.1; therefore, a lower bound of 0.1 was selected for $\kappa_{cell\text{-}cell}$.

To determine the amount of thermal strain applied to the cell elements and the cell-substrate contact stiffness, $\kappa_{cell\text{-}substrate}$, a parametric study was performed by matching the maximum and RMS of the tractions measured computationally to the tractions measured experimentally. It was found that a thermal strain value of −2.8 and a cell-substrate stiffness of $\kappa_{cell\text{-}substrate}$ = 0.2 matched both the maximum and RMS tractions to within ~5%, which indicated that the model captured the mechanics of cellular contraction on a compliant substrate reliably. A summary of all the model parameters and their values is given in Table 1.

RESULTS AND DISCUSSION

We use 3D TFM to measure the cell-generated traction stresses transmitted to the underlying substratum during EGF-mediated decompaction of an MCF-10A cell cluster. Representative tractions before and after stimulation with 100 ng/mL EGF are shown in Figs. 2 and 3, respectively. It is found that the cell clusters contract inward with most of the inward tractions applied at the periphery of the cell clusters. In addition, tractions in the out-of-plane direction are present. For all experiments performed, the RMS of the out-of-plane traction component is within a factor of 2 of the RMS of the in-plane traction components. These results emphasize the importance of 3D measurements of the tractions cells apply to a flat substrate. Although Figs. 2 and 3 show results from only one trial, the results discussed here are observed for all of the experiments performed.

By considering the RMS tractions from $n = 3$ trials before and after stimulation with 100 ng/mL EGF, it is found that the magnitude of the 3D traction vector increases by a factor of (mean ± standard deviation) 1.3 ± 0.2 30 min after stimulation. Ninety minutes after stimulation (data not shown), the relative change in tractions is found to reduce to 1.0 ± 0.2, indicating that the effect of the EGF begins to wear off after 90 min. In contrast, it is found that treatment with 0.1 ng/mL EGF (data not shown) does not

TABLE 1 Parameters used in the finite element simulations of a cluster of cells contracting on a linear, elastic substrate

Parameter	Value
Substrate Young's modulus ($E_{substrate}$)	7.1 kPa
Substrate Poisson's ratio ($\nu_{substrate}$)	0.48
Cell cluster Young's modulus (E_{cell})	1 kPa
Cell cluster Poisson's ratio (ν_{cell})	0.3
Cell-cell dimensionless adhesion stiffness ($\kappa_{cell\text{-}cell}$)	0.1 and 1
Cell-substrate dimensionless adhesion stiffness ($\kappa_{cell\text{-}substrate}$)	0.2
Thermal strain	−2.8

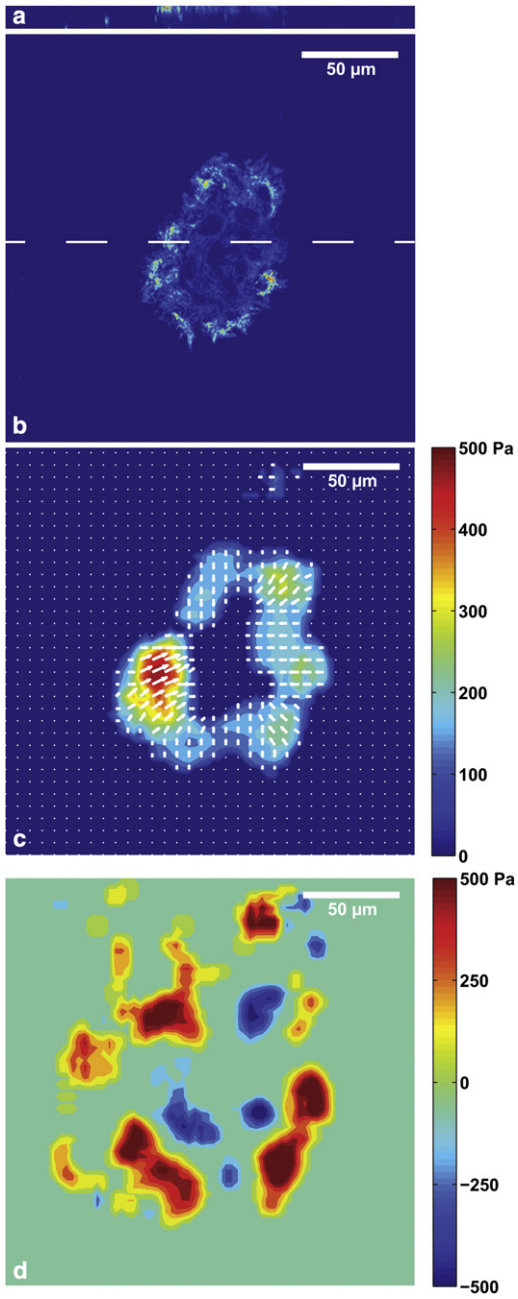

FIGURE 2 Tractions applied by a representative MCF-10A cell cluster to the polyacrylamide substrate measured with 3D TFM before stimulation with EGF. (*a* and *b*) False color confocal image of the cell cluster in the *x-z* and *x-y* planes, respectively. The *x-z* plane chosen in *a* is indicated by the dotted line in (*b*). The size scales for *a* and *b* are identical. (*c*) In-plane traction magnitudes (*colors*, *online*) and directions (*vectors*). (*d*) Out-of-plane traction component. Positive indicates the cell cluster pulls upward on the substrate. The out-of-plane traction component is as large as the in-plane components. In addition, the out-of-plane traction components show that the cells pull upward at the periphery of the cluster and push downward just inside the periphery, generating a local traction moment. Although the data shown here are for only one cell cluster, the qualitative results are the same for the other cell clusters studied. The viewing areas in *b*, *c*, and *d* are identical.

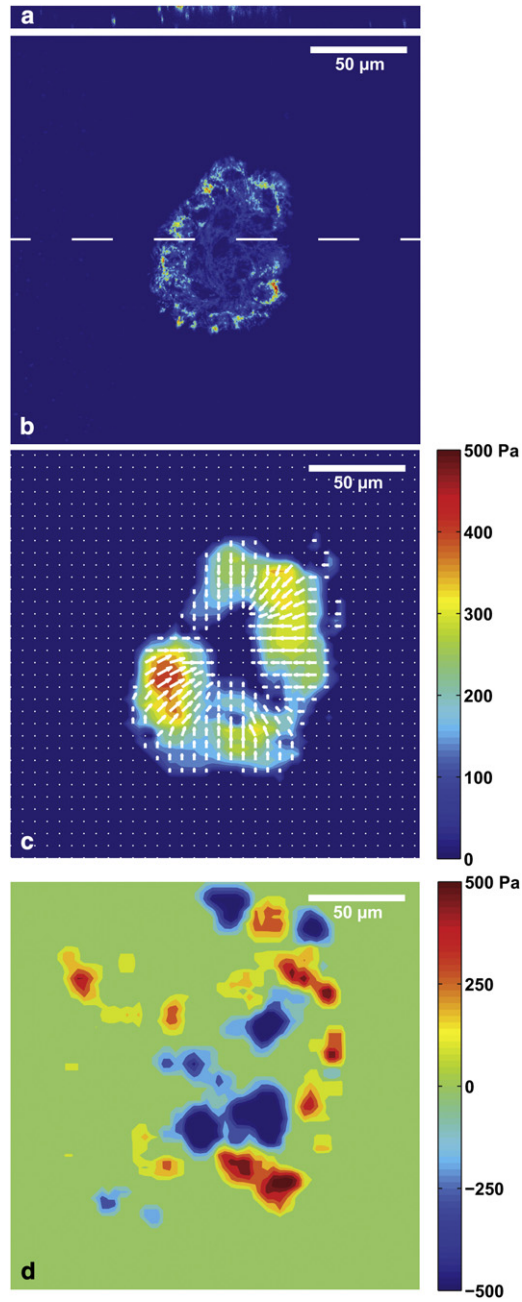

FIGURE 3 Tractions applied by the same MCF-10A cell cluster shown in Fig. 2 30 min after stimulation with 100 ng/mL EGF. (*a* and *b*) False color confocal image of the cell cluster in the *x-z* and *x-y* planes, respectively. The size scales for *a* and *b* are identical. (*c*) In-plane traction magnitudes (*colors*, *online*) and directions (*vectors*). (*d*) Out-of-plane traction component. A qualitative comparison of the tractions to those before stimulation with EGF (Fig. 2) shows little difference. The viewing areas in *b*, *c*, and *d* are identical.

produce a measureable change in tractions at either the 30 or 90 min time points. It has been shown previously that treatment with a high level of EGF (100 ng/mL) caused contact-inhibited interior cells to enter into the cell cycle, leading to a uniform proliferation pattern within epithelial cell clusters

(4). Because cellular tractions have been shown to affect cellular proliferation (23), it is possible that high levels of EGF may eliminate pre-EGF patterns of cell-substrate adhesion, thus generating larger cellular tractions to the substrate at the center of the cluster and stimulating uniform cell proliferation. However, the data show that the qualitative patterns of cell-substrate adhesion do not differ drastically before (Fig. 2) and after (Fig. 3) stimulation with EGF; therefore, it is more likely that high concentrations of EGF do not directly affect patterns in cell-substrate adhesion but instead induce uniform proliferation by over-riding downstream inhibitory pathways or providing compensatory activation pathways of proliferation.

In addition to a qualitative comparison of the tractions before and after EGF stimulation, the out-of-plane (z) component of the tractions (Figs. 2 *d* and 3 *d*) provides an important hint as to how the MCF-10A clusters behave mechanically. In addition to the fact that that the cell clusters apply tractions in the out-of-plane direction, it appears that the cell clusters apply tractions upward at the periphery of the cluster and downward inside the periphery of the cluster, forming a local traction moment on the substrate. This observation remains the same even after stimulation with EGF. This type of traction moment in the out-of-plane direction has been observed previously for 3D traction measurements of single cells on a flat substrate (24). Therefore, it is likely that the cells in the clusters operate cooperatively as a single unit to apply these traction patterns before and after stimulation with EGF.

To better understand whether cells act cooperatively as a single unit, a finite element simulation is used to investigate how cell-cell adhesion affects the tractions that clusters of cells apply to a flat substrate. The FE model used here extends previous finite element studies on cell clusters (23) by using linear springs at the locations of cellular adhesions to study adhesion strength. Like the experimental data, the simulation computes tractions that tend to pull the substrate inward in the in-plane directions (see Figs. 4 *a* and 5 *a*). In addition, the simulation predicts large tractions in the out-of-plane direction (Figs. 4 *b* and 5 *b*), which highlights the importance of 3D TFM measurements for a full understanding of cellular mechanical behavior. These out-of-plane tractions result from a bending deformation of the contractile layer (i.e., the cell cluster), which pulls upward at the periphery of the cluster. To maintain force equilibrium in the cluster, the cells push downward inside the periphery.

By changing the stiffness of the springs, it is possible to investigate the effect that changing the adhesion strength has on the tractions applied by the cell cluster to the substrate. As shown in Fig. 4 *b*, it is found that using the upper bound of the dimensionless cell-cell contact stiffness, $\kappa_{cell\text{-}cell} = 1$, (indicating a high level of cell-cell adhesion) produces an upward traction at the periphery of the cluster and a downward traction just inside of the upward traction,

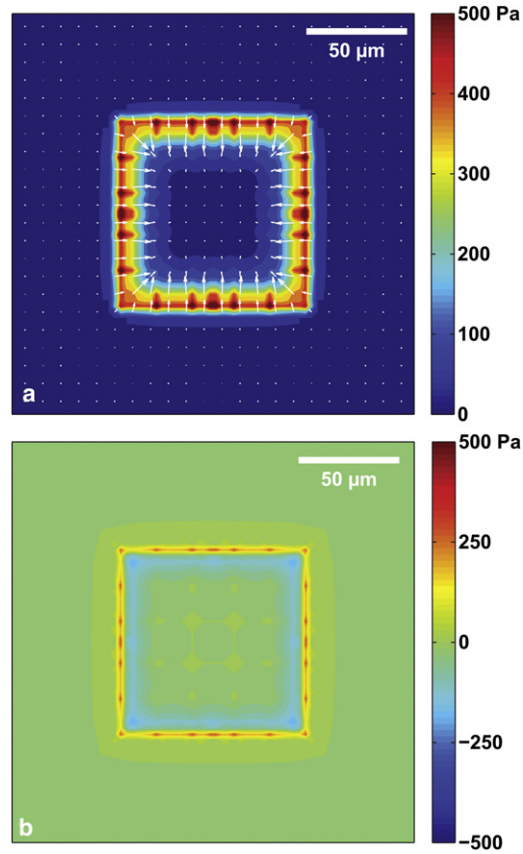

FIGURE 4 Finite element simulation of tractions applied by a well-adhered cluster of cells ($\kappa_{cell\text{-}cell} = 1$, $\kappa_{cell\text{-}substrate} = 0.2$). (*a*) The in-plane traction magnitudes (*color*, *online*) and directions (*vectors*) indicate the cluster pulls inward. (*b*) The out-of-plane traction component is upward at the periphery of the cell cluster and downward just inside the periphery, forming a similar traction moment as in Figs. 2 *d* and 3 *d*.

which forms a local moment similar to what is observed experimentally. This matching of the traction moment indicates that the model captures the mechanics involved in the contraction of a cluster of cells on a flat, compliant substrate. Together with the experimental data, this simple finite element simulation demonstrates that the cells in a cluster act cooperatively.

To further understand how the cells adhere to each other, the FE model is used to simulate the effect that reducing the cell-cell contact stiffness from the upper bound of $\kappa_{cell\text{-}cell} = 1$ to the lower bound of $\kappa_{cell\text{-}cell} = 0.1$ has on the tractions applied by the cell cluster to the polyacrylamide substrate. The results for the reduced contact stiffness ($\kappa_{cell\text{-}cell} = 0.1$) are shown in Fig. 5. Although the in-plane traction components (Fig. 5 *a*) do not differ from the model with a higher contact stiffness (Fig. 4 *a*), a comparison of Figs. 4 *b* and 5 *b* shows that the out-of-plane tractions do differ. The large fluctuations in out-of-plane traction magnitudes in Fig. 5 *b* are not observed experimentally either before (Fig. 2 *d*) or after stimulation with EGF (Fig. 3 *d*); therefore, we conclude that the MCF-10A cells maintain

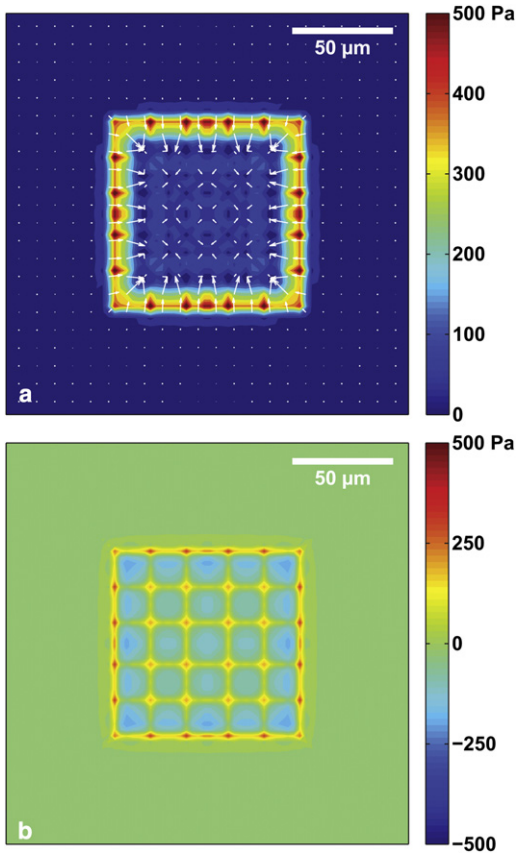

FIGURE 5 Simulated tractions applied by a loosely-adhered cluster of cells ($\kappa_{cell\text{-}cell} = 0.1$, $\kappa_{cell\text{-}substrate} = 0.2$). (*a*) The in-plane traction magnitudes (*color*, *online*) and directions (*vectors*) indicate the cluster pulls inward as in Fig. 4 *a*. (*b*) The out-of-plane traction component does not show the local traction moment observed experimentally (Figs. 2 *d* and 3 *d*). In addition, the out-of-plane traction shows more fluctuation than for well-adhered cells (Fig. 4 *b*).

strong cell-cell adhesions before and after stimulation with EGF. To verify that this conclusion is independent of the cell-substrate contact stiffness, $\kappa_{cell\text{-}substrate}$, a parametric study is conducted using values of $\kappa_{cell\text{-}substrate}$ ranging from 0.05 to 1 (Fig. S1, Supporting Material). It is found in the parametric study that the general trends discussed here do not change when the cell-substrate contact stiffness is changed, indicating the robustness of the FE model. Taking together the results of the experiments and the finite element simulation, we conclude that EGF does not directly reduce the cell-cell adhesion strength in MCF-10A clusters on a substrate with a Young's modulus of 7.1 kPa.

The previous conclusions have used 3D TFM experimental data to quantify the effects of EGF on the tractions in an MCF-10A cell cluster. The importance of the 3D data in this experiment cannot be overstated—it is from the out-of-plane (z) component of the traction vector that most of the observations are made. The FE model created to better understand the data also show tractions in the out-of-plane (z) direction. The results of the FE model can be further analyzed to underscore the importance of traction measurements in 3D. In-plane (x-y) traction components applied by cells with a high level of cell-cell adhesion ($\kappa_{cell\text{-}cell} = 1$) and a low level of cell-cell adhesion ($\kappa_{cell\text{-}cell} = 0.1$) are shown in Figs. 4 *a* and 5 *a*, respectively. Because the simulated cellular behavior is drastically different, a simple qualitative comparison of these two figures shows little difference between the in-plane traction magnitudes and distributions. A more quantitative analysis reveals that the in-plane traction magnitudes for a cluster with $\kappa_{cell\text{-}cell} = 1$ (Fig. 4 *a*) fluctuate between 0 and 15 Pa inside the periphery of the cluster. In comparison, the in-plane traction magnitudes for a cluster with $\kappa_{cell\text{-}cell} = 0.1$ (Fig. 5 *a*) fluctuate between 0 and 55 Pa. Although this difference in traction fluctuation may seem significant, it is below the noise floor of the experiment, which at 1% strain is equal to 71 Pa. Therefore, if one were to measure the tractions shown in Figs. 4 *a* and 5 *a* experimentally using two-dimensional (2D) TFM, it would not be possible to distinguish between the tractions applied by cells that are tightly adhered to each other and the tractions applied by cells that are loosely adhered to each other. On the other hand, the fluctuation in the out-of-plane traction component when $\kappa_{cell\text{-}cell} = 0.1$ (Fig. 5 *b*) is between 0 and 200 Pa. This fluctuation is above the noise floor of 71 Pa; therefore, if such a fluctuation were present in the experiments, it would be observed using the 3D techniques employed here. Because our measurements of cellular tractions do not show this type of fluctuation in the out-of-plane traction component either before or after stimulation, the conclusion that there is no change in the distribution of out-of-plane tractions is verified.

To better understand the reason that a 2D TFM measurement cannot resolve the difference between cells adhering tightly and loosely to one another, consider the hypothetical system of two cells interacting with each other as shown in Fig. 6. In Fig. 6 *a*, the cells are tightly adhered to each other; therefore, at the location of adhesion, they apply minimal tractions to the substrate beneath them. In contrast, Fig. 6 *b* shows a pair of cells that do not adhere to each other, but instead they adhere to the substrate beneath them. Here, the cells apply tractions to the substrate in the in-plane (*horizontal*) direction and out-of-plane (*vertical*) direction. However, at the location between the cells, the displacements caused by the in-plane tractions that the cells apply cancel each other out by the mechanical principle of superposition, so no displacements can be observed by a 2D TFM experiment. This issue of traction superposition causing zero net displacement should be considered in any TFM experiment involving multiple cells or cell clusters, especially the experiments that use a traction imbalance within the cell cluster to measure cell-cell tractions (25,26). On the basis of this analysis, we conclude that the best way to verify that cells are well-adhered to each other is by observing the out-of-plane traction component in addition to the in-plane traction components. If an experimenter

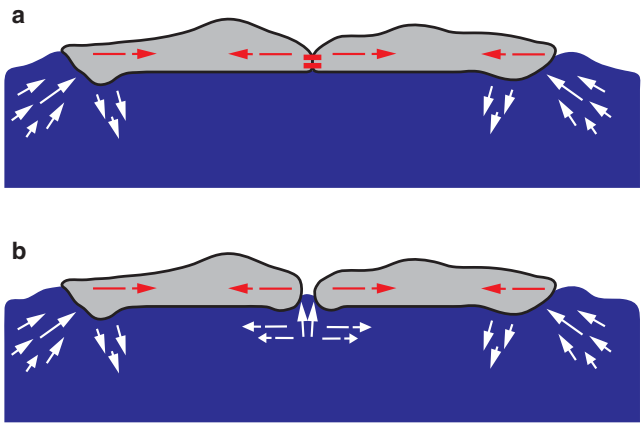

FIGURE 6 (*Color online*) Illustration of the importance of out-of-plane traction measurements in a multicellular system. In (*a*) the cells are well adhered (as indicated by the *red bars* at the location of cell-cell contact) and apply tractions to the substrate primarily at their outer edges, generating substrate displacements (*white arrows*) at their outer edges. In *b* the cells are not adhered, so they apply tractions at both their outer edges and the intercellular space. However, in-plane (*horizontal*) substrate displacements in the intercellular space are nearly zero, because the in-plane tractions applied by the cells cancel (as indicated by the *dashed white arrows*). In contrast, the out-of-plane (*vertical*) displacements in the intercellular space are nonzero.

measures only in-plane tractions, extra care must then be taken to ensure that the spatial resolution and traction sensitivity are sufficiently high to measure gradients in traction at the length scale of the cell-cell junctions.

CONCLUSIONS

3D TFM is employed to measure the tractions applied by epithelial cell clusters to a compliant substrate before and after stimulation with EGF. It is found that EGF increases the magnitude of the tractions within the cell cluster but does not change the distribution of tractions. A simple FE model is developed to better understand the mechanics of a cluster of cells adhering to one another and to the substrate beneath them. Together with the experimental observation that the spatial distribution of tractions applied by the cluster does not change before and after stimulation with EGF, the FE model gives evidence that EGF does not directly reduce the level of cell-cell adhesion present in a cell cluster. This result has implications in the study of processes associated with EMT-like behavior such as cell cluster decompaction and cell scattering.

The FE model developed here also demonstrates the importance of 3D measurements, especially in multicellular systems. Specifically, the FE model shows that a simple 2D in-plane measurement would not be able to accurately capture a reduction in cell-cell adhesion strength by a cluster of cells, because the in-plane tractions do not change by a measureable amount as the cell-cell adhesion strength decreases. Therefore, due to the increasing popularity of TFM and the interest in multicellular systems, 3D traction measurement techniques should be considered for future studies.

SUPPORTING MATERIAL

A figure is available at http://www.biophysj.org/biophysj/supplemental/S0006-3495(12)00218-4.

This research was supported by grants from the National Science Foundation (Division of Materials Research No. 0520565) through the Center for Science and Engineering of Materials at the California Institute of Technology to G.R. and A.R.A. and the National Institutes of Health (R01-CA138899 and U54CA143907) to A.R.A. J.N. was supported by the Department of Defense through the National Defense Science and Engineering Graduate Fellowship Program.

REFERENCES

1. Debnath, J., and J. S. Brugge. 2005. Modelling glandular epithelial cancers in three-dimensional cultures. *Nat. Rev. Cancer.* 5:675–688.
2. Engler, A. J., P. O. Humbert, …, V. M. Weaver. 2009. Multiscale modeling of form and function. *Science.* 324:208–212.
3. Kim, J. H., and A. R. Asthagiri. 2011. Matrix stiffening sensitizes epithelial cells to EGF and enables the loss of contact inhibition of proliferation. *J. Cell Sci.* 124:1280–1287.
4. Kim, J. H., K. Kushiro, …, A. R. Asthagiri. 2009. Tunable interplay between epidermal growth factor and cell-cell contact governs the spatial dynamics of epithelial growth. *Proc. Natl. Acad. Sci. USA.* 106:11149–11153.
5. Kalluri, R., and R. A. Weinberg. 2009. The basics of epithelial-mesenchymal transition. *J. Clin. Invest.* 119:1420–1428.
6. de Rooij, J., A. Kerstens, …, C. M. Waterman-Storer. 2005. Integrin-dependent actomyosin contraction regulates epithelial cell scattering. *J. Cell Biol.* 171:153–164.
7. Lee, M. Y., C. Y. Chou, …, M. R. Shen. 2008. Epithelial-mesenchymal transition in cervical cancer: correlation with tumor progression, epidermal growth factor receptor overexpression, and snail up-regulation. *Clin. Cancer Res.* 14:4743–4750.
8. Dise, R. S., M. R. Frey, …, D. B. Polk. 2008. Epidermal growth factor stimulates Rac activation through Src and phosphatidylinositol 3-kinase to promote colonic epithelial cell migration. *Am. J. Physiol. Gastrointest. Liver Physiol.* 294:G276–G285.
9. Schneider, I. C., C. K. Hays, and C. M. Waterman. 2009. Epidermal growth factor-induced contraction regulates paxillin phosphorylation to temporally separate traction generation from de-adhesion. *Mol. Biol. Cell.* 20:3155–3167.
10. Lilien, J., and J. Balsamo. 2005. The regulation of cadherin-mediated adhesion by tyrosine phosphorylation/dephosphorylation of beta-catenin. *Curr. Opin. Cell Biol.* 17:459–465.
11. Hoschuetzky, H., H. Aberle, and R. Kemler. 1994. Beta-catenin mediates the interaction of the cadherin-catenin complex with epidermal growth factor receptor. *J. Cell Biol.* 127:1375–1380.
12. Gladden, A. B., A. M. Hebert, …, A. I. McClatchey. 2010. The NF2 tumor suppressor, Merlin, regulates epidermal development through the establishment of a junctional polarity complex. *Dev. Cell.* 19: 727–739.
13. Mitic, L. L., and J. M. Anderson. 1998. Molecular architecture of tight junctions. *Annu. Rev. Physiol.* 60:121–142.
14. Franck, C., S. Hong, …, G. Ravichandran. 2007. Three-dimensional full-field measurements of large deformations in soft materials using confocal microscopy and digital volume correlation. *Exp. Mech.* 47:427–438.
15. Lucy, L. B. 1974. Iterative technique for rectification of observed distributions. *Astron. J.* 79:745–754.

16. Dembo, M., and Y. L. Wang. 1999. Stresses at the cell-to-substrate interface during locomotion of fibroblasts. *Biophys. J.* 76:2307–2316.

17. Del Alamo, J. C., R. Meili, …, J. C. Lasheras. 2007. Spatio-temporal analysis of eukaryotic cell motility by improved force cytometry. *Proc. Natl. Acad. Sci. USA.* 104:13343–13348.

18. Reference deleted in proof.

19. Janmey, P. A., and C. A. McCulloch. 2007. Cell mechanics: integrating cell responses to mechanical stimuli. *Annu. Rev. Biomed. Eng.* 9:1–34.

20. Deshpande, V. S., R. M. McMeeking, and A. G. Evans. 2007. A model for the contractility of the cytoskeleton including the effects of stress-fibre formation and dissociation. *Proc. R. Soc. A.* 463:787–815.

21. Dembo, M., D. C. Torney, …, D. Hammer. 1988. The reaction-limited kinetics of membrane-to-surface adhesion and detachment. *Proc. R. Soc. of Lond. B Bio. Sci.* 234:55–83.

22. Ward, M. D., and D. A. Hammer. 1993. A theoretical analysis for the effect of focal contact formation on cell-substrate attachment strength. *Biophys. J.* 64:936–959.

23. Nelson, C. M., R. P. Jean, …, C. S. Chen. 2005. Emergent patterns of growth controlled by multicellular form and mechanics. *Proc. Natl. Acad. Sci. USA.* 102:11594–11599.

24. Maskarinec, S. A., C. Franck, …, G. Ravichandran. 2009. Quantifying cellular traction forces in three dimensions. *Proc. Natl. Acad. Sci. USA.* 106:22108–22113.

25. Maruthamuthu, V., B. Sabass, …, M. L. Gardel. 2011. Cell-ECM traction force modulates endogenous tension at cell-cell contacts. *Proc. Natl. Acad. Sci. USA.* 108:4708–4713.

26. Tambe, D. T., C. C. Hardin, …, X. Trepat. 2011. Collective cell guidance by cooperative intercellular forces. *Nat. Mater.* 10:469–475.